
Article:
Cunningham, V.J., Giakoumatos, E.C., Ireland, P.M. et al. (3 more authors) (2017) Giant Pickering droplets: effect of nanoparticle size and morphology on stability. Langmuir, 33 (31). pp. 7669-7679. ISSN 0743-7463

https://doi.org/10.1021/acs.langmuir.7b01383

LANGMUIR

Article

Giant Pickering droplets: effect of nanoparticle size and morphology on stability

Victoria Jane Cunningham, Emma C. Giakoumatos, Peter Matthew Ireland, Charlotte J Mable, Steven P Armes, and Erica J. Wanless

Langmuir, **Just Accepted Manuscript** • DOI: 10.1021/acs.langmuir.7b01383 • Publication Date (Web): 15 Jul 2017

Langmuir is published by the American Chemical Society. 1155 Sixteenth Street N.W., Washington, DC 20036

Giant Pickering droplets: effect of nanoparticle size and morphology on stability

Victoria J. Cunningham,[a] Emma C. Giakoumatos,[b$] Peter M. Ireland,[b] Charlotte J. Mable,[a] Steven P. Armes[a]* and Erica J. Wanless[b]*

a. Department of Chemistry, University of Sheffield, Brook Hill, Sheffield, South Yorkshire, S3 7HF, UK

b. Priority Research Centre for Advanced Particle Processing and Transport, University of Newcastle, Callaghan, NSW, 2308, Australia.

$ current address: Institute of Complex Molecular Systems, Eindhoven University of Technology, The Netherlands (e.giakoumatos@tue.nl)

* Corresponding authors: Erica.wanless@newcastle.edu.au and s.p.armes@shef.ac.uk

Abstract

The interaction between a pair of millimeter-sized nanoparticle-stabilized *n*-dodecane droplets was analyzed by high-speed video camera. The droplets were grown in the presence of either poly(glycerol monomethacrylate)-poly(benzyl methacrylate) (PGMA-PBzMA) diblock copolymer spheres or poly(glycerol monomethacrylate)-poly(2-hydroxypropyl methacrylate)-poly(benzyl methacrylate) (PGMA-PHPMA-PBzMA) triblock copolymer worms prepared by polymerization-induced self-assembly (PISA). The effect of nanoparticle morphology on droplet coalescence was analyzed by comparing 22 nm spheres to highly anisotropic worms with a mean worm width of 26 nm and comparable particle contact angle. Both morphologies lowered the interfacial tension, providing direct evidence for nanoparticle adsorption at the oil-water interface. At 0.03 % w/v copolymer, at least 90 seconds was required to stabilize the *n*-dodecane droplets in the presence of the worms, whereas no ageing was required to produce stable droplets when using the spheres, suggesting faster diffusion of the latter to the surface of the droplets. The enhanced stability of the sphere-coated droplets is consistent with the higher capillary pressure in this system as the almost planar interfaces approach. However, the more strongly adsorbing worms ultimately also confer stability. At lower copolymer concentrations (≤ 0.01% w/v) worm adsorption promoted droplet stability, whereas the spheres were unable to stabilize droplets even after longer ageing times. The effect of mean sphere diameter on droplet stability was also assessed while maintaining an approximately constant particle contact angle. Small spheres of either 22 nm or 41 nm stabilized *n*-dodecane droplets, whereas larger spheres of either 60 or 91 nm were unable to prevent coalescence when the two droplets were brought into contact. These observations are consistent with the greater capillary pressure stabilizing the oil-water interfaces coated with the smaller spheres. Addition of an oil-soluble polymeric diisocyanate cross-linker to either the 60 nm or the 91 nm spheres produced highly stable colloidosomes, thus confirming adsorption of these nanoparticles.

Introduction

Although their existence has been known for more than a century, particle-stabilized (or Pickering) emulsions have enjoyed something of a renaissance over the past sixteen years. This belated activity has been inspired by fundamental studies by Binks,[1-6] as well as many other workers.[7-12] Many types of particles can be used to prepare Pickering emulsions, with the emulsion type being dictated primarily by the surface wettability rather than the specific surface chemistry. Literature examples of Pickering emulsifiers include silica,[6,10] various latexes,[8,11,13,14] proteins,[15] clay platelets,[16,17] gold sols,[12] quantum dots,[18] carbon black[19] and graphene.[7,20] Compared to surfactant-stabilized emulsions, Pickering emulsions offer reduced foaming, minimal skin irritation and more reproducible formulations.[2] These advantages have led to renewed commercial interest in such systems for industrial sectors such as pharmaceutics,[21,22] cosmetics[23-25] and agrochemicals.[26,27] Moreover, a better fundamental understanding of Pickering emulsions is critical for the development of more effective methods to destabilize petroleum emulsions.[28,29]

In principle, millimeter-sized pendent oil droplets coated in adsorbed particles offer a useful model system for understanding the behavior of conventional Pickering emulsions.[30] Firstly, monitoring the dynamic interfacial tension of a single pendent droplet can be used to infer the particle adsorption kinetics and hence establish the minimum equilibration times required for droplet coalescence studies.[31] Investigation of the interaction and stability against coalescence of a pair of droplets when brought into close contact permits characterization of the intervening thin film stability.[32] Upon droplet approach, the effectively irreversibly adsorbed particles[2,33] inhibit thin film drainage.[34] However, using smaller particles or particles with higher contact angles yield thinner films upon close approach of droplet pairs and thus a reduced steric barrier towards coalescence. A second potential contributor to film stability, albeit with an opposing geometric component is the capillary pressure, which serves to stabilize the interfaces on close approach. Here, as the particle radius is reduced, the radius of curvature of the adjacent liquid-liquid interface is reduced proportionally, and the capillary pressure is thus increased. As summarized by Kaptay,[35] an unstable film is the result of a 'tipping point' mechanism when the film thins beyond the point where the capillary force is maximized (see Figure S1 in the Supporting Information). Collapse then occurs on a timeframe determined by hydrodynamics. For a fixed particle contact angle of 60 to 90°, using *smaller* particles creates a greater capillary barrier to film collapse. This will tend to allow more stable particle-stabilized thin films (or droplets) to be prepared for a given film thickness. As thus envisioned, the stability of particle-stabilized thin films is a delicate balance between the adsorption energy of the particles which increases with particle size, and the capillary pressure afforded by the adsorbed particles which is inversely proportional to particle size.

If the particle-stabilized thin film is unstable, the mechanism of droplet coalescence in a Pickering emulsion is via particle bridging between the two droplet interfaces.[36,37] Such coalescence events can be prevented by either the formation of a close-packed monolayer or bilayer contact between approaching droplets.[35] These alternative particle organizations during thin film drainage were inferred by studying the stability of *n*-dodecane or sunflower oil droplets stabilized by poly(glycerol monomethacrylate) (PGMA) stabilized polystyrene (PS) latexes of either 135 or 902 nm diameter.[38] In this study, all pairs of Pickering droplets proved to be unstable with respect to coalescence on close approach, which was attributed to their relatively low radii of curvature. Notably, droplet coalescence could be prevented by covalently cross-linking the latex particles via their steric

stabilizer chains using an oil-soluble polymeric diisocyanate. Giant Pickering droplets coated with 260 nm poly(tert-(butylamino)ethyl methacrylate) (PTBAEMA) latexes also coalesced on close contact.[31] From these prior studies of millimeter-sized Pickering droplets, it is unclear whether the droplet (in)stability stems principally from the aqueous film thickness formed upon contact, the size of the adsorbed particles or the droplet surface coverage.

Over the last decade, polymerization-induced self-assembly (PISA) has become widely recognized as a versatile, efficient and robust technique for the rational synthesis of block copolymer nanoparticles.[39-42] Aqueous PISA formulations are particularly attractive, with many reports describing the use of reversible addition-fragmentation chain transfer (RAFT) aqueous emulsion polymerization.[43-55] Such protocols enable the production of sterically-stabilized spherical nanoparticles at relatively high solids (up to 50% w/w copolymer). Of particular relevance to the present work, a PGMA chain transfer agent (CTA) can be chain-extended using benzyl methacrylate (BzMA) to produce a range of PGMA-PBzMA diblock copolymer spheres of 28 to 230 nm diameter.[56] These model nanoparticles can be used to prepare Pickering emulsions with mean droplet diameters of up to 1000 μm via high shear homogenization using oils such as *n*-dodecane or sunflower oil. In related work, Mable and co-workers recently reported the chain extension of a water-soluble poly(glycerol monomethacrylate)-poly(2-hydroxypropyl methacrylate) (PGMA-PHPMA) diblock copolymer precursor with BzMA to produce well-defined PGMA-PHPMA-PBzMA triblock copolymer worms.[57] Such worms were reported by Thompson et al. to be more effective Pickering emulsifiers compared to their spherical counterparts.[58] For a fixed copolymer concentration of 0.06% w/v, the PGMA-PHPMA-PBzMA triblock copolymer worms yielded significantly smaller (~ 200 μm) oil-in-water Pickering emulsion droplets compared to PGMA-PBzMA spheres (~ 400 μm droplets). The greater droplet diameter obtained for the sphere-stabilized Pickering emulsions is consistent with the higher capillary pressure present in this system; this parameter scales with the nanoparticle curvature and is therefore halved in the case of the adsorbed worms.

In the present work, we examine a series of four PGMA-PBzMA spheres ranging in mean diameter from 22 to 91 nm and also the above PGMA-PHPMA-PBzMA worms as putative emulsifiers for the Pickering stabilization of isolated millimeter-sized *n*-dodecane droplets. This enabled the effect of both particle size and morphology on droplet stability to be assessed at a fixed contact angle for the first time using high-speed video imaging and dynamic interfacial tensiometry.

Experimental

Synthesis of $PGMA_{37}$-$PHPMA_{60}$-$PBzMA_{30}$ Worms

The $PGMA_{37}$-$PHPMA_{60}$-$PBzMA_{30}$ triblock copolymer worms were prepared via RAFT seeded emulsion polymerization. Full details of this PISA synthesis have been reported previously.[57,58] More than 99% monomer conversion was achieved for the synthesis of both the diblock copolymer precursor and the triblock copolymer worms as judged by ^{1}H NMR spectroscopy. The $PGMA_{37}$ macro-CTA, $PGMA_{37}$-$PHPMA_{60}$ diblock copolymer precursor and the $PGMA_{37}$-$PHPMA_{60}$-$PBzMA_{30}$ triblock copolymer were analyzed by DMF GPC analysis, see Figure S2a. A mean worm core width of 26 nm was determined by TEM by measuring at least 30 nanoparticles using ImageJ software.

Synthesis of $PGMA_{39}$-$PBzMA_x$ spherical nanoparticles

$PGMA_{39}$-$PBzMA_x$ diblock copolymer nanoparticles were prepared via RAFT emulsion polymerization of BzMA at 70 °C and 10% w/w solids utilizing a $PGMA_{39}$ macro-CTA which had been previously purified by precipitation in dichloromethane. The target degree of polymerization of the hydrophobic PBzMA block was varied from 60 to 300. Full details of this synthesis protocol have been reported previously.[56] A summary of the characterization details for the various diblock copolymer nanoparticles used in this study is given in Table 1. High conversions (> 99%) were achieved for all syntheses. The $PGMA_{39}$ macro-CTA and the four corresponding diblocks were analyzed by DMF gel permeation chromatography (GPC) analysis using a series of near-monodisperse poly(methyl methacrylate) (PMMA) calibration standards, see Figure S2b. The hydrodynamic number-average diameter determined by DLS is utilized throughout as this is the most relevant parameter for interfacial packing at the oil droplet surface. TEM studies were performed using a Philips CM100 instrument operating at 100 kV and equipped with a Gatan 1 k CCD camera. Aqueous nanoparticle dispersions (0.20% w/w) were adsorbed onto carbon-coated TEM grids for 60 s and then stained with uranyl formate (0.75% w/w) for 20 s prior to imaging. A comparison between the DLS and TEM diameters for the various copolymer nanoparticles is provided in Figure S3.

Sample preparation

The nanoparticle dispersions used in this work were required to be of sufficiently low turbidity to ensure capture of high-quality video images. For example, to prepare a 0.03 % w/v dispersion of 22 nm $PGMA_{39}$-$PBzMA_{60}$ nanoparticles, 156 µL of the original 9.61 % w/w copolymer dispersion was added to a beaker containing Milli-Q water (50 mL). This was stirred for 20 min prior to droplet growth. Concentrations of 0.06 % w/v, 0.09 % w/v and 0.13 % w/v were used for the 41, 60 and 91 nm spheres, respectively. These three concentrations ensure the same interfacial coating ability for each dispersion, that is, an equivalent total projected interfacial area to that of the 0.03 % w/v 22 nm sphere dispersion (see Table 1). A concentration of 0.03 % w/v was also used for the experiments conducted using the $PGMA_{37}$-$PHPMA_{60}$-$PBzMA_{30}$ worms.

Droplet Coalescence Apparatus

A schematic representation of the apparatus used in this work is shown in Figure S4 and was reported previously for studying the coalescence of pairs of air bubbles[32,59] or oil droplets.[31,38,60] Two stainless steel capillaries (1.05 mm outer diameter) were inserted into a glass beaker containing 50 mL of an aqueous nanoparticle dispersion and a magnetic stirrer bar. The capillary tips were visually aligned in x, y and z directions in order to minimize any prospect of lateral shear-induced coalescence when the droplets approach.[61,62] Two microsyringe pumps (Sarasota, FL) were used to produce two identical *n*-dodecane droplets from the tips of the capillaries. Between experiments, all glassware, syringes, capillaries and the stirrer bar were thoroughly cleaned using 2-propanol and ethanol to remove any oily residues and then rinsed with Millipore Milli-Q water at least ten times to remove residual contaminants. Coalescence data were recorded using a high-speed video camera (Phantom 5, Vision Research, USA) at a rate of 1800 frames·s^{-1}. Images were collected using Phantom 6.30 (Nikon) software at 512 × 256 resolution.

Droplet Coalescence Protocol and Data Analysis

n-Dodecane was held in both syringes and then connected to the capillaries. All air bubbles were expelled from the capillaries prior to their addition to the aqueous phase. The beaker containing the aqueous dispersion and a magnetic stirrer (or in the absence of any nanoparticles for the bare oil droplet experiments) was placed inside a rectangular Perspex vessel containing water to prevent optical distortion arising from the cylindrical surface of the beaker. The beaker was then placed on a magnetic stirrer mounted on a lab jack beneath the capillaries. 2.0 mL of *n*-dodecane was added to the top of the water surface. This was required to maintain a constant surface area of the oil throughout the experiment. Oil droplets of approximately 2.0 mm diameter were then grown from the capillaries. During droplet ageing, the aqueous phase was stirred magnetically. One of the capillaries was then moved using a linear actuator at 0.238 cm s^{-1} until the two droplets were just touching (no visible intervening aqueous film). The droplet coalescence time was measured from the point of initial droplet contact until coalescence as analyzed from the video footage. Each coalescence experiment was conducted at least three times (except when 20 min ageing was required; in this case only two experiments were performed) and the mean and standard deviation for the coalescence time was recorded. The projected droplet surface area before and after coalescence was measured as a function of time. The droplet area in each frame was analyzed using ImageJ software and the results were plotted as the change in projected area relative to the initial droplet area prior to coalescence.

Cross-linking experiments

For the cross-linking experiments, the same protocol was followed as described above, except that the pure *n*-dodecane in the syringes was replaced with a solution containing 0.10 mg/mL 2,4-diisocyanate-terminated poly(propylene glycol) (PPG-TDI, Sigma Aldrich) cross-linker dissolved in *n*-dodecane.

Pendent Drop Tensiometry

Interfacial tensions were measured for single pendant 10 µL *n*-dodecane droplets suspended in Milli-Q water and also aqueous dispersions of either spherical or worm-like nanoparticles using a PAT-1 tensiometer (SINTERFACE Technologies, Berlin, Germany). A nanoparticle concentration of 0.03 % w/v was used to compare the 22 nm $PGMA_{39}$-$PBzMA_{60}$ spheres with the $PGMA_{37}$-$PHPMA_{60}$-$PBzMA_{30}$ worms. Concentrations of 0.01 % w/v, 0.02 % w/v, 0.03 % w/v and 0.04 % w/v were used for the 22, 41, 60 and 91 nm spheres, respectively (these conditions were selected to maintain an equivalent projected surface area while ensuring each dispersion was used at sufficiently low turbidity). The data presented are the mean and standard deviation from three experiments. The density of these dilute aqueous nanoparticle dispersions was assumed to be that of pure water (1.00 $g{\cdot}cm^{-3}$) and the density of *n*-dodecane was taken to be 0.75 $g{\cdot}cm^{-3}$ (Sigma Aldrich).

Results and Discussion

Effect of adsorbed particle morphology

The synthesis of amphiphilic diblock copolymers via PISA has enabled the rational design of a wide range of bespoke nanoparticles, including both spherical and worm-like micelles.[39-42] In this study, RAFT emulsion polymerization was utilized to prepare $PGMA_{37}$-$PHPMA_{60}$-$PBzMA_{30}$ triblock copolymer worms using a water-soluble $PGMA_{37}$-$PHPMA_{60}$ diblock copolymer precursor (Table 1) and $PGMA_{39}$-$PBzMA_{60}$ spheres using a water-soluble $PGMA_{39}$ macro-CTA (Table 1). The PGMA macro-CTAs were purified via precipitation to remove small molecule contaminants. Syntheses of the diblock and triblock copolymers each proceeded to high conversions (> 99%) as judged by ^{1}H NMR spectroscopy, while GPC analysis (Figure S2) indicated low dispersity polymers with high blocking efficiencies relative to the PGMA macro-CTA. TEM studies confirmed that the worms are well-defined in terms of their mean width, which is comparable to the mean diameter of the $PGMA_{39}$-$PBzMA_{60}$ spheres. However, the worms are relatively polydisperse in terms of their length, see Figure 1, because 1D sphere-sphere fusion during PISA is the mechanism by which spheres form worms.[41] Previously, Thompson et al. reported that both PGMA-PBzMA spheres and PGMA-PHPMA-PBzMA triblock copolymer worms can stabilize oil-in-water Pickering emulsions, where *n*-dodecane was used as the model oil.[58] The worms proved to be more effective Pickering emulsifiers than the spheres since finer oil droplets were obtained when using the same mass of copolymer. This was attributed to the worms being much more strongly adsorbed at the oil-water interface than the spheres as a result of the far greater energy of attachment in the former case.

Table 1. DLS, conversions, solids content, concentration used for coalescence experiments and TEM analysis of $PGMA_{39}$-$PBzMA_x$ diblock copolymer spheres and a $PGMA_{37}$-$PHPMA_{60}$-$PBzMA_{30}$ triblock copolymer worm.

	Block composition	Conv. (d_7-DMF)	Solids content[a]	DLS		TEM		Concentration (% w/v)
				Num. Av.	PDI	Diameter	Morphology	
1	G_{37}-H_{60}-B_{30}	>99%	13.0 %	78 nm[b]	0.19	26 nm	Worms	0.005 - 0.03
2	G_{39}-B_{60}	>99%	9.6%	22 nm	0.07	25 nm	Spheres	0.01 – 0.05
3	G_{39}-B_{125}	>99%	9.5%	41 nm	0.02	42 nm	Spheres	0.06
4	G_{39}-B_{200}	>99%	9.8%	60 nm	0.05	60 nm	Spheres	0.09
5	G_{39}-B_{300}	>99%	9.8%	91 nm	0.05	83 nm	Spheres	0.13

a. solids content determined by moisture analysis, b. z-average particle diameter.

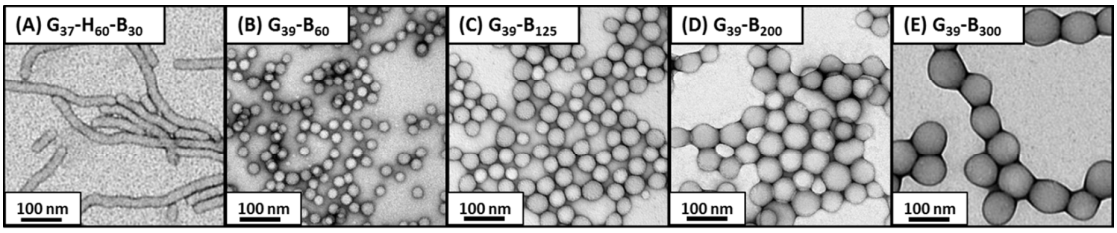

Figure 1. Transmission electron microscopy images for either $PGMA_{37}$-$PHPMA_{60}$-$PBzMA_{30}$ worms or $PGMA_{39}$-$PBzMA_x$ spheres (where x = 60, 125, 200 and 300).

In the present study, a copolymer concentration of 0.03 % w/v was initially selected to ensure that the bulk concentration remained essentially constant after nanoparticle adsorption at the oil-water interfaces (droplets plus top coating of aqueous dispersion). Moreover, this copolymer concentration was sufficiently low to minimize turbidity and hence enable visual examination of droplet stability with respect to coalescence. The oil selected for the current giant Pickering emulsion study was *n*-dodecane to enable direct comparison with earlier work by both Thompson et al.[58] and Cunningham et al.,[56] who prepared conventional Pickering emulsions with similar nanoparticles. The spheres and worms comprise either a $PGMA_{37}$ or a $PGMA_{39}$ stabilizer block. Thus these two types of nanoparticles should, to a good first approximation, exhibit essentially the same contact angle at the *n*-dodecane-water interface, enabling the effect of copolymer morphology to be assessed. The stability of millimeter-sized oil-in-water Pickering emulsion droplets has been previously investigated by Thompson et al.[38] and Morse et al.,[31] but neither a worm-like morphology nor particles of less than 100 nm diameter has been studied to date.

Dynamic interfacial tension is a convenient technique to assess the kinetics of particle adsorption at the oil-water interface prior to studying the coalescence behavior of giant Pickering droplets. Initially, the interfacial tension of a bare *n*-dodecane droplet in water was measured for 10 min (see Figure 2). An equilibrium interfacial tension of 44.8 ± 1.9 $mN{\cdot}m^{-1}$ was established within 10 min, which is comparable to that reported by Thompson et al. (47.2 ± 2.9 $mN{\cdot}m^{-1}$).[38] The interfacial tension of *n*-dodecane droplets grown in the presence of 0.03 % w/v nanoparticle dispersions of either the 22 nm $PGMA_{39}$-$PBzMA_{60}$ spheres or the $PGMA_{37}$-$PHPMA_{60}$-$PBzMA_{30}$ worms were also recorded over a 10 min period. Both spheres and worms exhibited a rapid initial reduction in interfacial tension within the first 20 s, with a more gradual but still significant reduction thereafter. In principle, such a reduction might indicate the presence of low molecular weight surface-active species. However, in practice assessment of the supernatants of dialyzed nanoparticles indicated limited evidence for this problem, as shown in Figure 2 for the 22 nm spheres. Therefore, these observations confirm nanoparticle adsorption at the oil-water interface,[63] and perhaps suggest some degree of post-adsorption reorganization. Interestingly, the worms lower the interfacial tension significantly more than the spheres; the former produce a final interfacial tension of 21.7 ± 0.3 $mN{\cdot}m^{-1}$ compared to a limiting value of 27.7 ± 0.4 $mN{\cdot}m^{-1}$ for the latter. This suggests that the worms have a stronger affinity for the *n*-dodecane-water interface than the spheres.

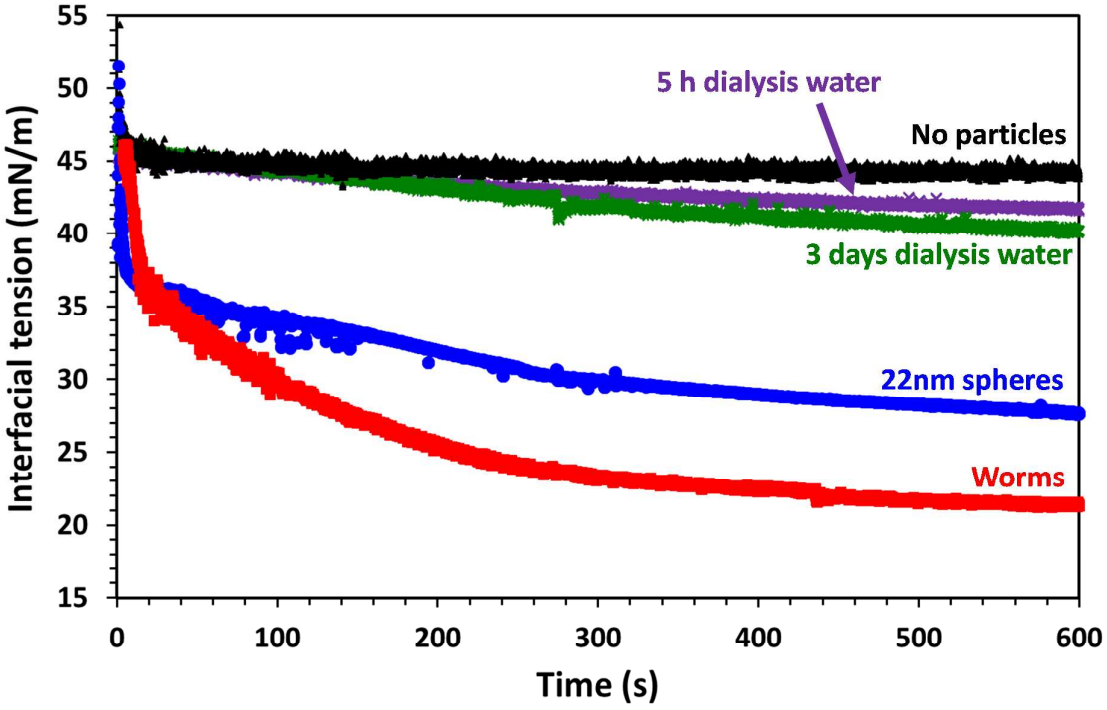

Figure 2. Interfacial tension profiles obtained for *n*-dodecane droplets grown in unstirred 0.03% w/v aqueous dispersions of either 22 nm $PGMA_{39}$-$PBzMA_{60}$ spheres or $PGMA_{37}$-$PHPMA_{60}$-$PBzMA_{30}$ worms of comparable mean width and aged for 10 min. Also shown is a reference for *n*-dodecane in water in the absence of any nanoparticles, together with the interfacial tensions determined for the dialysate after dialyzing a dispersion of the 22 nm spheres for either 5 h or 3 days.

These 22 nm spheres and highly anisotropic worms were subsequently used to prepare giant-Pickering emulsions, see Scheme 1. The stability of two millimeter-sized *n*-dodecane droplets towards coalescence was examined by studying droplet coalescence as a function of droplet ageing time. First, bare *n*-dodecane droplets were studied: a pair of *n*-dodecane droplets were grown in MilliQ water and brought into contact. Instantaneous coalescence occurred, as expected for a clean non-stabilized system. The coalescence times observed for the 0.03% w/v aqueous dispersions of either $PGMA_{39}$-$PBzMA_{60}$ spheres or $PGMA_{37}$-$PHPMA_{60}$-$PBzMA_{30}$worms were determined for various ageing times (Figure 3). The *ageing time* is defined as the time between growing the droplets and bringing them into contact, whereas the *coalescence time* is the time between initial contact of the two droplets and the onset of coalescence. Thus an ageing time of zero seconds indicates that the droplets are grown and immediately brought into contact. For the current set-up, this typically takes 10 – 15 s and applies to all ageing times presented herein.

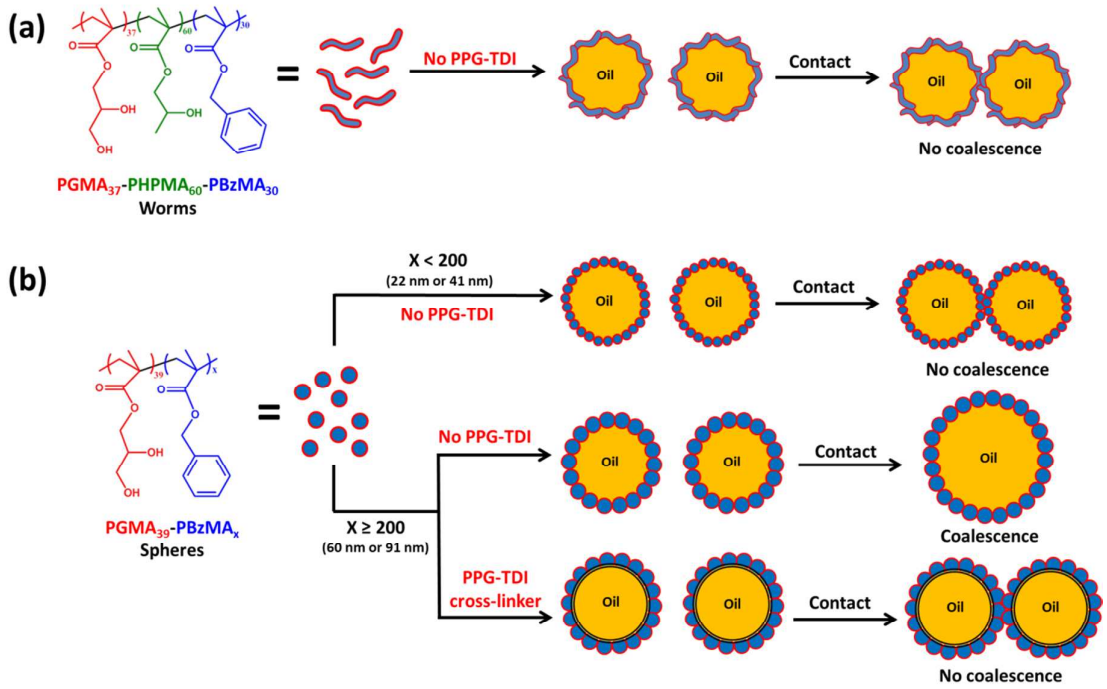

Scheme 1. Reaction scheme for the formation of giant Pickering emulsion droplets: (a) using $PGMA_{37}$-$PHPMA_{60}$-$PBzMA_{30}$ triblock copolymer worms and (b) using $PGMA_{39}$-$PBzMA_x$ diblock copolymer spheres. With sufficient ageing prior to direct contact, the worms are able to stabilize the emulsion droplets. Stability could be induced with minimal ageing in dispersions of spheres of either 22 nm or 41 nm diameter, whereas *n*-dodecane droplets exposed to 60 nm or 91 nm diameter spheres always coalesced on contact, regardless of the ageing time. Addition of an oil-soluble cross-linker, poly(propylene glycol) tolyl diisocyanate (PPG-TDI), to the droplet phase produces robust colloidosomes that resist coalescence.

Using the 22 nm $PGMA_{39}$-$PBzMA_{60}$ spheres at 0.03% w/v led to a measurable degree of droplet stability within ageing times of 0 - 30 s. This suggests that a sufficient number of spheres adsorb onto the pair of *n*-dodecane droplets during their growth, i.e. with minimal interfacial ageing, to produce enhanced stability towards coalescence. These observations were not expected, because Thompson et al. reported that significantly larger PGMA-stabilized polystyrene latexes of either 135 nm or 902 nm were unable to stabilize equivalent millimeter-sized *n*-dodecane droplets even after droplet ageing times of up to 2 min.[38] In contrast, the $PGMA_{39}$-$PBzMA_{60}$ spheres can rapidly stabilize at least some pairs of droplets. This suggests relatively fast diffusion and attachment to the expanding oil-water interface, which is consistent with the rapid initial reduction in interfacial tension shown in Figure 2. If the particle contact angle at the *n*-dodecane-water interface is comparable for the nanoparticles and the latexes, then the enhanced droplet stability can be explained by the larger capillary pressure ($\propto$ 1/R) sustained by the smaller nanoparticles.[35] The unexpected ability of 22 nm $PGMA_{39}$-$PBzMA_{60}$ spheres to stabilize millimeter-sized Pickering droplets is consistent with previous work by Cunningham et al., who utilized 41 nm $PGMA_{51}$-$PBzMA_{100}$ spheres to prepare unusually large Pickering emulsions (up to 1 mm diameter) using high-shear homogenization.[56]

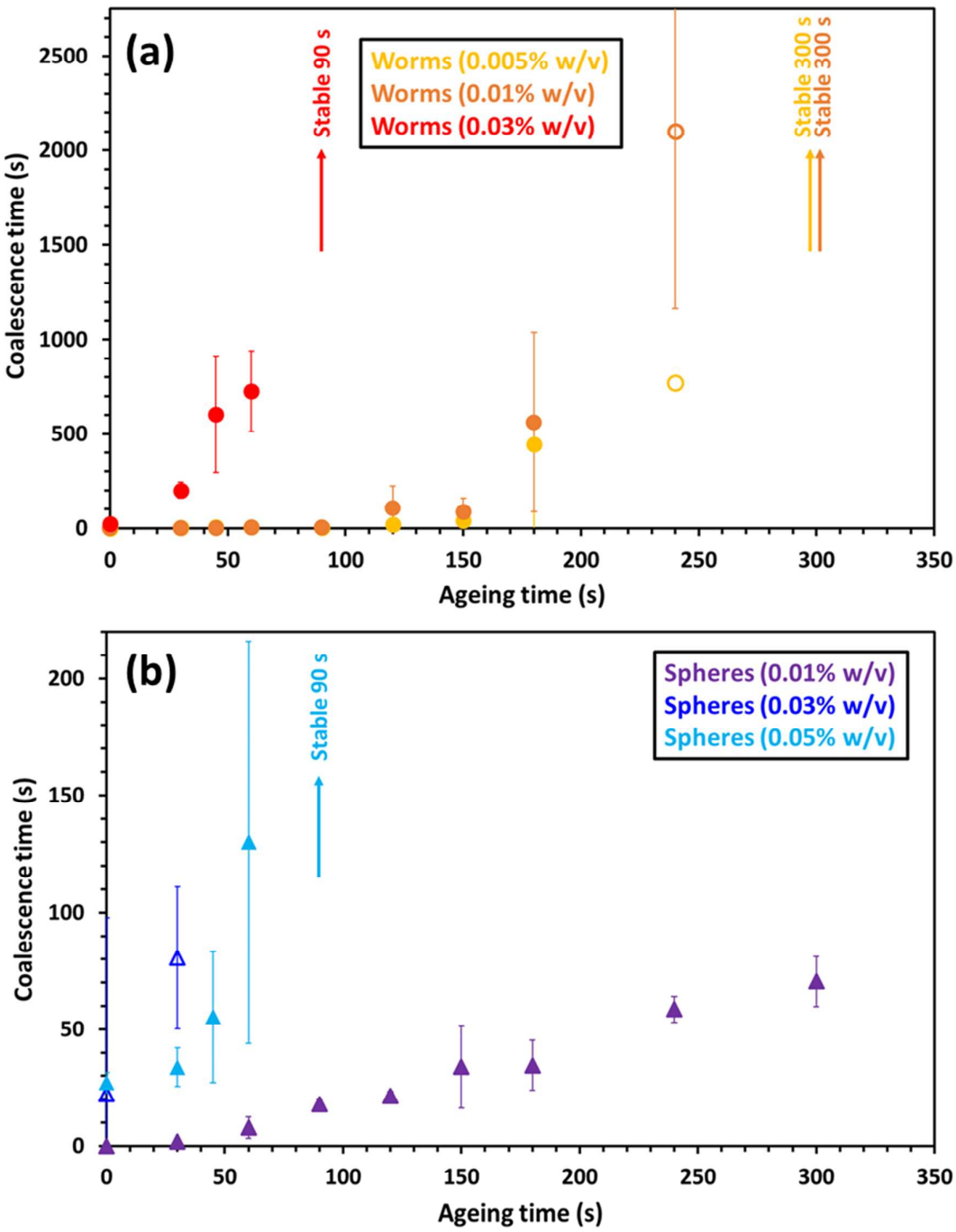

Figure 3. Coalescence time for two *n*-dodecane droplets recorded after various ageing times for (a) worms and (b) 22 nm spheres at differing copolymer concentrations. Open symbols indicate conditions for which some droplets remained stable for at least 30 min in contact while coalescence occurred for other droplets; the error bars indicate variability in the data for repeat measurements.

In contrast, using the worms at 0.03% w/v produced inferior droplet stability in the absence of ageing, followed by a significant increase in droplet coalescence time with ageing time (Figure 3). This is consistent with longer ageing times facilitating higher levels of nanoparticle adsorption at the surface of each droplet (Figure 2). Initially, the aqueous thin film between the two droplets is less stable as the capillary pressure is approximately half that present with the adsorbed spherical nanoparticles (which have double the mean curvature compared to the worms). After 90 s ageing (with stirring), the worm-coated droplets became stable towards coalescence. This indicates that the larger worms require longer to coat the droplet surface than the relatively small, faster diffusing spheres. Moreover, after initial contact with the oil-water interface, the worms should adsorb conformally so as to maximize their contact area and hence minimize the surface area of the new interface. This may lead to defects in the adsorbed layer. The 22 nm $PGMA_{39}$-$PBzMA_{60}$ spheres are sufficiently small that their energy of detachment will be relatively low, which may enable these nanoparticles to rapidly rearrange (or perhaps even desorb and readsorb) at the droplet surface. This dynamic situation ultimately produces a hexagonal close-packed layer, minimizes surface defects and results in stable droplets being produced more quickly than for the worms. A conventional Pickering emulsion droplet prepared by homogenization of *n*-dodecane with a 0.50% w/v dispersion of the 22 nm spheres was imaged by TEM (see Figure S5). Inspection of the flattened dried droplet indicates areas of hexagonally close-packed spheres that suggest efficient nanoparticle packing at the *n*-dodecane-water interface prior to drying. However, the high shear homogenization technique used to prepare bulk emulsions facilitates faster delivery of the nanoparticles to the interface compared to the approximately diffusion-controlled conditions present in the coalescence rig (which only utilizes gentle stirring).

The droplet coalescence behavior in the 0.03% w/v aqueous dispersions was captured using a high-speed video camera recording 1800 frames per second. Figure 4a and 4b show every fifth frame from the onset of coalescence for both the spheres and the worms after an ageing time of 30 s in each case. Initially, the aqueous thin film between the two contacting droplets ruptures to form a thick neck, see image 2 (t = 1.1 ms). The resulting oil droplet then continues to expand horizontally, leading to a larger relative projected surface area for the coalescing droplets (Figure 4c). The droplet then contracts horizontally and its vertical height increases. This oscillatory motion repeats with a reduction in expansion in both planes being observed over time as a result of energy dissipation in the system. Finally, the larger droplet reaches equilibrium. The presence of either spheres or worms induces a time lag compared to the behavior of bare *n*-dodecane droplets in water. The coalescence dynamics of worm-stabilized *n*-dodecane droplets are noticeably slower compared to those of the sphere-stabilized droplets. This phase lag is evident in the images shown in Figure 4a and 4b, where image 4 recorded for the spheres after 8.3 ms has the same droplet shape as that of image 5 (recorded after 11.1 ms) for the worm-stabilized droplets. Any overlap of the adsorbed worms would be likely to hinder the change in surface area associated with the coalescing droplet and result in the slower dynamics shown in Figure 4c. The differing dynamics shown in Figure 4c were assessed using a simple harmonic oscillator model to monitor the change in projected area over time to determine a damping coefficient.[64] A damping coefficient of 0.024 ms^{-1} was recorded for bare *n*-dodecane droplets in water after 30 s ageing. Both the sphere-coated and worm-coated droplets exhibited equivalent damping coefficients with 0.025 ms^{-1} being determined for the former system and 0.024 ms^{-1} for the latter. Usually, a higher damping coefficient implies greater rigidity and robustness for the Pickering droplets.[64] However, the adsorbed nanoparticles only seem to affect the phase lag.

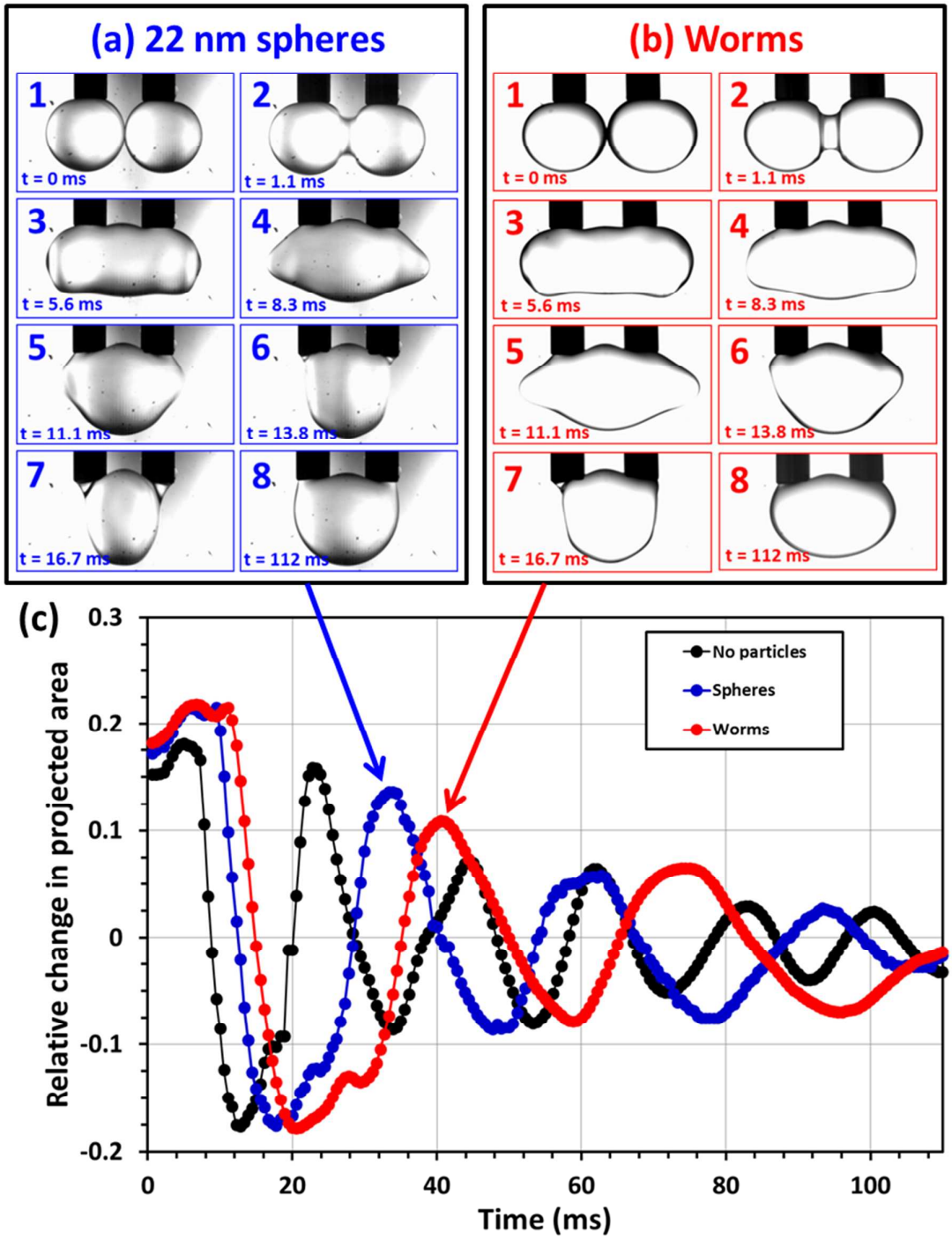

Figure 4. Sequence of images recorded for a pair of coalescing *n*-dodecane droplets grown in a 0.03% w/v aqueous dispersion after 30 s ageing: (a) 22 nm $PGMA_{39}$-$PBzMA_{60}$ spheres and (b) $PGMA_{37}$-$PHPMA_{60}$-$PBzMA_{30}$ worms. (c) Coalescence dynamics observed for bare *n*-dodecane droplets (no particles, black trace), 22 nm diameter $PGMA_{39}$-$PBzMA_{60}$ spheres (blue trace) and $PGMA_{37}$-$PHPMA_{60}$-$PBzMA_{30}$ worms (red trace). In each case the outer diameter of each capillary was 1.05 mm.

The effect of copolymer concentration on the coalescence behavior was studied for both the worms and 22 nm spheres, see Figure 3. As the worms produced stable droplets after 90 s ageing at a copolymer concentration of 0.03% w/v, two lower concentrations (0.005% w/v and 0.01% w/v) were also examined, Figure 3a. An increase in coalescence time with ageing time was observed in both cases. Partial stability occurred after ageing for 4 min, with complete stability being obtained after 5 min ageing. This is physically reasonable: lower copolymer concentrations should require longer ageing times to allow more worms to adsorb at and/or rearrange on the droplet surface. Similarly, the 22 nm spheres were studied at varying concentrations, Figure 3b. In this case, only partial stability was observed at 0.03% w/v. Hence, a higher concentration (0.05% w/v) and a lower concentration (0.01% w/v) were selected for further study. The latter condition produced a longer coalescence time with increasing ageing time, but these droplets never became fully stable towards coalescence. This result was somewhat unexpected, because using worms at the same copolymer concentration produces stable droplets despite a thirty-fold reduction in the number of nanoparticles present in solution. In contrast, using 0.05% w/v spheres yielded longer coalescence times with increasing ageing time, with indefinitely stable droplets being formed after 90 s ageing. For both nanoparticle morphologies, higher copolymer concentrations prevent coalescence. Furthermore, comparing the coalescence data shown in Figure 3, both the 0.05% w/v spheres and 0.03% w/v worms require an ageing time of 90 s to produce stable droplets under otherwise identical conditions. This suggests that the worms have a greater affinity for the droplet surface, enabling stability to be achieved at a lower concentration than that required for the 22 nm spheres.

Thompson et al. reported that $PGMA_{37}$-$PHPMA_{60}$-$PBzMA_{30}$ worms were more strongly adsorbed at the oil droplet surface than $PGMA_{39}$-$PBzMA_{60}$ spheres in Pickering emulsions. The former nanoparticles also produced smaller oil droplets when employed at the same copolymer concentration. These observations suggest that worms are more effective Pickering emulsifiers than the near-equivalent spheres.[58] Hence the present study focused on whether worms also offer significant advantages over spheres for the preparation of giant (~ 2 mm diameter) Pickering emulsions at various copolymer concentrations. On a relatively short timescale, spheres diffuse faster and hence adsorb more quickly at the droplet surface than the larger worms. This is supported by interfacial tension studies (unstirred) as well as droplet stability measurements (stirred) and can be explained by the very high capillary pressure present in the aqueous thin film stabilized by these adsorbed spherical nanoparticles. Furthermore, worms lead to greater droplet stability if longer ageing times are utilized, suggesting that these nanoparticles require longer to fully coat and stabilize the oil droplets. Compared to spheres with a mean diameter comparable to that of the mean worm width, it is estimated that the energy of detachment for highly anisotropic worms is approximately 30-50 times greater.[58] One likely consequence is that the dynamics of adsorbed worms may be significantly slower than that of spheres, thus the former system requires longer time scales to produce the dense, uniform surface layer required to prevent droplet coalescence. In summary, both spheres and worms can stabilize giant Pickering droplets, but the former stabilize interfaces with lower curvature (i.e. larger droplets) more quickly than the latter.[58]

Effect of sphere diameter

Our previous studies suggested that adsorbed latex particles required chemical cross-linking in order to produce millimeter-sized Pickering emulsion droplets capable of resisting coalescence when brought into close contact.[31,38] However, the 22 nm $PGMA_{39}$-$PBzMA_{60}$ spheres confer droplet stability without any interparticle crosslinking (see Figure 3), while closely-related 41 nm $PGMA_{51}$-$PBzMA_{100}$ spheres can stabilize droplets with mean diameters as large as 1 mm for conventional emulsions prepared via high-shear homogenization.[56] The key parameter for such droplet stability appears to be the thin film maximum capillary pressure (see Figure S1). Moreover, both Thompson et al.[38] and Morse et al.[31] utilized substantially larger latexes and found the analogous giant Pickering droplets to be unstable towards coalescence, despite the thicker aqueous thin films between the contacting droplets. The PGMA-PS latexes examined by Thompson et al. had mean diameters of 135 nm and 902 nm, whereas a 260 nm diameter PTBAEMA latex was used by Morse et al. Thus a series of PGMA-PBzMA spheres were targeted in which the mean degree of polymerization of the core-forming PBzMA block was systematically varied from 60 to 300 (Table 1). High conversions were achieved in each case, resulting in 41 nm, 60 nm and 91 nm spheres in addition to the 22 nm spheres described above (see Figure 1 for representative TEM images of these spheres). These nanoparticles cover the desired intermediate range of mean curvature.

In order to facilitate comparison between the interfacial stabilizing ability of the four different diameter spheres, some important assumptions and considerations are noteworthy. Firstly, the same $PGMA_{39}$ macro-CTA stabilizer was employed for each sphere synthesis, so these nanoparticles should exhibit approximately the same three-phase contact angle at the oil-water interface. Secondly, the increase in mean sphere diameter inevitably leads to greater turbidity in aqueous dispersions: this point must be considered when selecting suitable copolymer concentrations for visual analysis using the high-speed video camera. Indeed, this prevents any meaningful comparison at the same copolymer concentration based on the number of nanoparticles. Instead, the relative performance of these four types of spherical nanoparticles was compared using the total equivalent projected area of nanoparticles in each dispersion, which necessarily required a significantly higher concentration of the 91 nm spheres compared to the 22 nm spheres. Hence the equivalent interfacial surface area (assuming hexagonal close packing, see Figure S5) was used, as described by Thompson et al.[38]

The dynamic interfacial tension for each of the four spheres was measured over 10 min and compared to that of bare *n*-dodecane droplets in water (Figure 5). The concentration of 22 nm spheres was 0.01 % w/v, so concentrations of 0.02, 0.03 and 0.04 % w/v were used for the 41, 60 and 91 nm spheres respectively (see Table 2). All four nanoparticle dispersions effectively lowered the interfacial tension compared to the interfacial tension observed in the absence of any nanoparticles, providing strong evidence for nanoparticle adsorption at the oil-water interface. Despite the variation in particle diameter, an equilibrium surface tension of 35.6 ± 0.4 $mN{\cdot}m^{-1}$ was observed in each case (see Table 2). This suggests that each of the $PGMA_{39}$-$PBzMA_x$ spheres behave similarly at the oil-water interface provided that sufficient time is allowed for equilibration. Focusing on the first 80 s after the droplet is grown, the smallest spheres reduce the interfacial tension more quickly (see Figure 5 inset), while the largest spheres require the longest ageing time to reach equilibrium and intermediate behavior is observed for the 41 and 60 nm spheres. This is consistent

with the larger number of 22 nm spheres for the same equivalent projected surface area, leading to a higher probability of inelastic collisions during droplet growth.

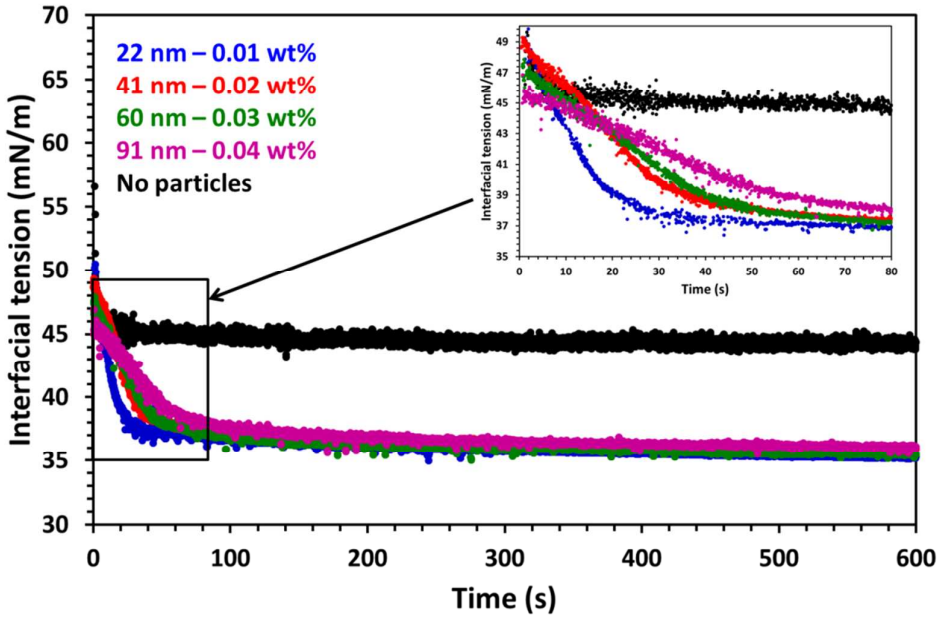

Figure 5. Interfacial tension profiles for *n*-dodecane droplets grown in unstirred aqueous dispersions of $PGMA_{39}$-$PBzMA_x$ spheres and aged for 10 min (where x = 60, 125, 200 and 300 for 22 nm, 41 nm, 60 nm and 91 nm diameter nanoparticles, respectively). The concentrations correspond to the equivalent interfacial area coating capacity of 22 nm spheres at 0.01% w/v (see Table 2). The black trace is a reference for *n*-dodecane droplets grown in pure water in the absence of any nanoparticles.

Table 2. Summary of particle diameter, copolymer concentration for interfacial tension measurements (IFT) and equilibrium IFT for the four $PGMA_{39}$-$PBzMA_x$ spheres used in this study.

Particle diameter	Copolymer concentration for IFT (% w/v)	Equilibrium IFT (mN/m)
22 nm	0.01	35.2 ± 0.3
41 nm	0.02	35.9 ± 0.1
60 nm	0.03	35.4 ± 0.3
91 nm	0.04	36.0 ± 0.3

The coalescence behavior of two giant *n*-dodecane droplets in each aqueous sphere dispersion was assessed at a concentration that resulted in an equivalent projected area to that of the 22 nm

spheres at 0.03 % w/v, or 9.16×10^{17} nm^2. Therefore concentrations of 0.06 % w/v, 0.09 % w/v and 0.13 % w/v were used for the 41, 60 and 91 nm spheres, respectively (see Table 1). Millimeter-sized *n*-dodecane droplets were grown in turn in the presence of each nanoparticle dispersion and the ageing time was systematically varied. The mean coalescence time versus ageing time for the four sets of nanoparticles is shown in Figure 6. Both the 22 nm and 41 nm spheres produced either stable or partially stable droplets (i.e. some droplets coalesced, whereas others remain stable for at least 30 min) when employing ageing times of just 45 s. However, no droplet stability was observed when using either the 60 or 91 nm spheres. Ageing times of up to 20 min were examined but droplet coalescence was invariably observed in all cases. This indicates that droplet coalescence is remarkably sensitive to the mean nanoparticle diameter in the range investigated as summarized in Scheme 1.

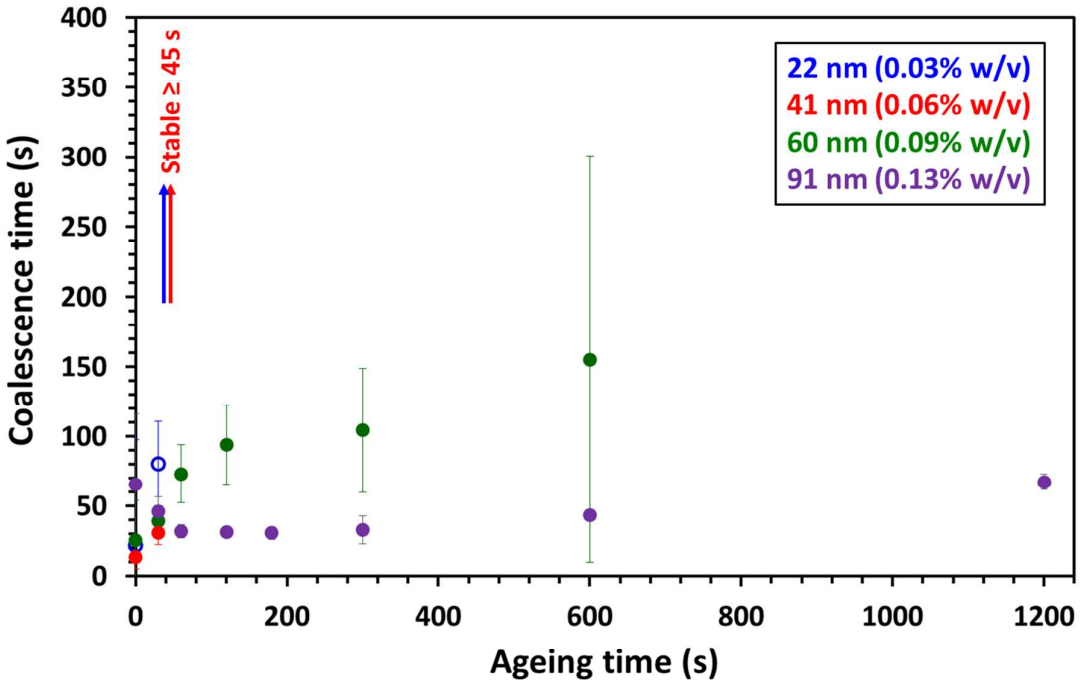

Figure 6. Coalescence time versus ageing time for two *n*-dodecane droplets grown in dilute aqueous dispersions of $PGMA_{39}$-$PBzMA_x$ spheres of varying mean diameter. The copolymer concentrations used correspond to the equivalent interfacial area coating capacity. Open markers indicate conditions where, in some cases, droplets were stable from coalescence for at least 30 min.

The post-coalescence behavior of the four sets of spheres was analyzed, see Figure S6. An ageing time of 30 s was selected, as this corresponded to the longest ageing time when coalescence was observed for all four sphere diameters. A similar phase lag was observed for the majority of the nanoparticles. A slightly larger damping coefficient with increasing particle diameter is observed, but all damping coefficients lie between 0.025 and 0.030 ms^{-1} and hence differ only slightly to that observed for pure *n*-dodecane in water (0.024 ms^{-1}).

To examine whether the 60 nm and 91 nm spheres could provide sufficient coverage of the droplet interfaces to prevent coalescence, PPG-TDI cross-linker was added to the *n*-dodecane phase (0.1 mg/mL). PPG-TDI reacts with the hydroxyl groups on the collapsed PGMA stabilizer chains that are in direct contact with the oil phase, cross-linking neighboring nanoparticles at the oil-water interface to yield stable colloidosomes.[65] The PPG-TDI molecule is estimated to have a maximum extended length of 15 nm,[38] therefore both the 60 nm and 91 nm nanoparticles must be sufficiently close-packed on the *n*-dodecane surface to enable cross-linking between adjacent nanoparticles (as opposed to cross-linking between PGMA stabilizer chains within individual nanoparticles). PPG-TDI-loaded oil droplets were grown in the presence of either 60 or 91 nm spheres and brought into contact after various ageing times, see Figure 7 and Scheme 1. Thompson et al. reported that an ageing time of 20 min was required to ensure droplet stability when using relatively large PGMA-PS latexes. In contrast, much shorter times were required for the smaller PGMA-PBzMA spheres used herein.[38] After just 5 min ageing, the 60 nm spheres prevented droplet coalescence, while only 2 min ageing was required for the 91 nm spheres to ensure droplet stability. This indicates the formation of stable colloidosomes via adsorption of the 60 and 91 nm spheres at the oil-water interface. For ageing times of less than 60 s, the incomplete (patchy) colloidosomes produced using the 60 or 91 nm spheres exhibited similar behavior to the Pickering emulsions prepared in the absence of any PPG-TDI cross-linker, and coalesced soon after contact. However, longer ageing times led to more robust colloidosomes with up to five times longer droplet coalescence times compared to the corresponding Pickering emulsions. In general, longer ageing times lead to more stable droplets. This is because more nanoparticles can adsorb at the oil-water interface to form a relatively close-packed monolayer and the PPG-TDI cross-linker has longer to react with the PGMA stabilizer chains to produce colloidosomes.[38]

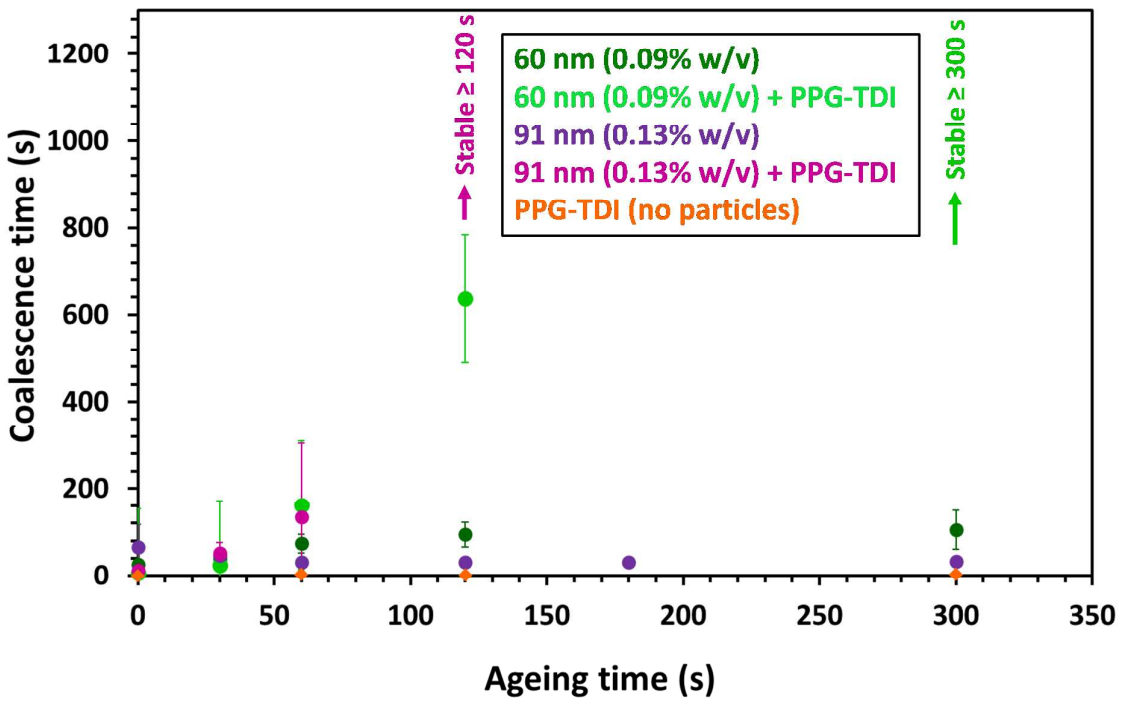

Figure 7. Coalescence time versus ageing time for a pair of *n*-dodecane droplets grown in an aqueous dispersion of either 60 nm diameter $PGMA_{39}$-$PBzMA_{200}$ spheres or 91 nm diameter $PGMA_{39}$-$PBzMA_{300}$ spheres, with and without the presence of 0.10 mg/mL PPG-TDI as a cross-linker. A control experiment was also conducted utilizing 0.1 mg/mL PPG-TDI in the absence of any nanoparticles. The copolymer concentrations utilized in these experiments correspond to the equivalent interfacial area coating capacity. The arrows indicate where the two droplets were stable to coalescence for at least 30 min.

These crosslinking experiments confirmed adsorption of all four spheres at the surface of the oil droplets, as supported by the interfacial tension data shown in Figure 5. Given that the sole variable within the study is the particle diameter, the differing stabilities of these nanoparticle-coated interfaces are consistent with the corresponding variation in the maximum sustainable capillary pressure, which scales with the mean curvature ($\propto 1/R$) for a fixed contact angle (as presented here). This is opposed by the aqueous film thickness which is proportional to the mean sphere diameter for a fixed three-phase particle contact angle. This balance yields a complex emulsion stability diagram for emulsions stabilized by a double layer of closely-packed nanoparticles, which is believed to be present in the above experiments.[35] In this context, Kaptay's analysis suggests markedly reduced emulsion stability for low curvature interfaces, which is the case for the giant Pickering droplets investigated herein.

Conclusions

The coalescence behavior of millimeter-sized *n*-dodecane droplets stabilized by $PGMA_{37}$-$PHPMA_{60}$-$PBzMA_{30}$ worms in aqueous solution was compared directly to that obtained for 22 nm diameter $PGMA_{39}$-$PBzMA_{60}$ spheres, which have comparable dimensions to the mean worm width. Both the spheres and worms adsorbed at the surface of the oil droplets, reducing the interfacial tension

relative to that of bare *n*-dodecane. Both spheres and worms were able to stabilize these giant Pickering emulsions. However, the 22 nm spheres proved to be more effective at stabilizing the interface in the absence of interfacial ageing, which was attributed to the very high capillary pressure generated by using such small nanoparticles. This is the first example of nanoparticle-stabilized giant Pickering emulsions. By comparison, the highly anisotropic worms required an ageing time of at least 90 s before droplet stability was observed, which is consistent with the somewhat slower adsorption and interfacial rearrangement/relaxation of such relatively massive particles. Analysis of droplet coalescence dynamics at 0.03% w/v after ageing times of 30 s revealed that the worm coated droplets exhibited a discernible time lag compared to that of either bare *n*-dodecane droplets or droplets prepared in the presence of the 22 nm spheres which is indicative of interfaces with restricted surface area changes. Systematic variation of the copolymer concentration revealed that the worms diffuse more slowly to the oil-water interface but are able to stabilize giant Pickering droplets at lower concentrations than the equivalent 22 nm spheres.

The effect of varying the sphere diameter on droplet coalescence behavior was also examined. $PGMA_{39}$-$PBzMA_x$ spheres of 22, 41, 60 and 91 nm diameter were compared at the same equivalent packing surface area. In each case the interfacial tension was lowered compared to bare *n*-dodecane droplets, suggesting nanoparticle adsorption at the oil-water interface. The relationship between coalescence time and ageing time indicated that stable droplets could be achieved when using the 22 nm and 41 nm spheres, but coalescence was always observed when employing the 60 nm and 91 nm spheres, even for relatively long ageing times of up to 20 min. Since all other parameters remained constant, this reduction in droplet stability with increasing nanoparticle diameter is attributed to the lower capillary pressure. Finally, addition of 0.1 mg/mL PPG-TDI crosslinker produced stable colloidosomes when using both the 60 nm and 91 nm spheres, which confirms that nanoparticle adsorption must occur in both cases.

Supporting Information

Thin film stability as a function of capillary pressure for contact angles of 60° and 90°. GPC data for the diblock copolymer spheres and triblock copolymer worms, TEM and DLS particle size measurements, a schematic representation of the coalescence apparatus, a TEM image of a dried Pickering emulsion droplet prepared using the 22 nm spheres together with the coalescence dynamics for coalescing *n*-dodecane droplets coated with the spherical nanoparticles. The Supporting Information is available free of charge on the ACS Publications website.

Acknowledgements

The EPSRC is thanked for a PhD studentship and Ashland is acknowledged for CASE support of VJC. The RSC and SCI are thanked for the Sir Eric Rideal travel bursary given to VJC that facilitated this international collaboration. M. Rymaruk is thanked for help with the dynamic interfacial tension measurements and cross-linker control experiments. Dr S. Ata and Dr G. Bournival are thanked for valuable discussions.

References

(1) Binks, B. P.; Lumsdon, S. O. Influence of Particle Wettability on the Type and Stability of Surfactant-Free Emulsions. *Langmuir* **2000**, *16*, 8622-8631.

(2) Binks, B. P. Particles as surfactants—similarities and differences. *Current Opinion in Colloid & Interface Science* **2002**, *7*, 21-41.

(3) Aveyard, R.; Binks, B. P.; Clint, J. H. Emulsions stabilised solely by colloidal particles. *Adv. Colloid Interface Sci.* **2003**, *100*, 503-546.

(4) Binks, B. P.; Clint, J. H. Solid wettability from surface energy components: relevance to Pickering emulsions. *Langmuir* **2002**, *18*, 1270-1273.

(5) Binks, B. P.; Whitby, C. P. Nanoparticle silica-stabilised oil-in-water emulsions: improving emulsion stability. *Colloids and Surfaces A: Physicochemical and Engineering Aspects* **2005**, *253*, 105-115.

(6) Binks, B. P.; Lumsdon, S. O. Catastrophic Phase Inversion of Water-in-Oil Emulsions Stabilized by Hydrophobic Silica. *Langmuir* **2000**, *16*, 2539-2547.

(7) McCoy, T. M.; Pottage, M. J.; Tabor, R. F. Graphene oxide-stabilized oil-in-water emulsions: pH-controlled dispersion and flocculation. *The Journal of Physical Chemistry C* **2014**, *118*, 4529-4535.

(8) Madivala, B.; Vandebril, S.; Fransaer, J.; Vermant, J. Exploiting particle shape in solid stabilized emulsions. *Soft Matter* **2009**, *5*, 1717-1727.

(9) Whitby, C. P.; Fornasiero, D.; Ralston, J. Effect of oil soluble surfactant in emulsions stabilised by clay particles. *Journal of Colloid and Interface Science* **2008**, *323*, 410-419.

(10) Whitby, C. P.; Fischer, F. E.; Fornasiero, D.; Ralston, J. Shear-induced coalescence of oil-in-water Pickering emulsions. *Journal of Colloid and Interface Science* **2011**, *361*, 170-177.

(11) Morse, A. J.; Dupin, D.; Thompson, K. L.; Armes, S. P.; Ouzineb, K.; Mills, P.; Swart, R. Novel Pickering Emulsifiers based on pH-Responsive Poly(tert-butylaminoethyl methacrylate) Latexes. *Langmuir* **2012**, *28*, 11742-11753.

(12) Duan, H.; Kuang, M.; Wang, D.; Kurth, D. G.; Möhwald, H. Colloidally Stable Amphibious Nanocrystals Derived from Poly{[2-(dimethylamino)ethyl] Methacrylate} Capping. *Angewandte Chemie International Edition* **2005**, *44*, 1717-1720.

(13) Thompson, K. L.; Chambon, P.; Verber, R.; Armes, S. P. Can Polymersomes Form Colloidosomes? *J. Am. Chem. Soc.* **2012**, *134*, 12450-12453.

(14) Fujii, S.; Read, E. S.; Binks, B. P.; Armes, S. P. Stimulus-Responsive Emulsifiers Based on Nanocomposite Microgel Particles. *Adv. Mater.* **2005**, *17*, 1014-1018.

(15) Murray, B. S.; Durga, K.; Yusoff, A.; Stoyanov, S. D. Stabilization of foams and emulsions by mixtures of surface active food-grade particles and proteins. *Food Hydrocolloids* **2011**, *25*, 627-638.

(16) Cui, Y.; Threlfall, M.; van Duijneveldt, J. S. Optimizing organoclay stabilized Pickering emulsions. *Journal of Colloid and Interface Science* **2011**, *356*, 665-671.

(17) Cui, Y.; van Duijneveldt, J. S. Microcapsules Composed of Cross-Linked Organoclay. *Langmuir* **2012**, *28*, 1753-1757.

(18) Skaff, H.; Lin, Y.; Tangirala, R.; Breitenkamp, K.; Böker, A.; Russell, T. P.; Emrick, T. Crosslinked capsules of quantum dots by interfacial assembly and ligand crosslinking. *Adv. Mater.* **2005**, *17*, 2082-2086.

(19) Van Hooghten, R.; Imperiali, L.; Boeckx, V.; Sharma, R.; Vermant, J. Rough nanoparticles at the oil–water interfaces: their structure, rheology and applications. *Soft Matter* **2013**, *9*, 10791-10798.

(20) He, Y.; Wu, F.; Sun, X.; Li, R.; Guo, Y.; Li, C.; Zhang, L.; Xing, F.; Wang, W.; Gao, J. Factors that Affect Pickering Emulsions Stabilized by Graphene Oxide. *Acs Applied Materials & Interfaces* **2013**, *5*, 4843-4855.

(21) Binks, B. P.; Fletcher, P. D. I.; Johnson, A. J.; Elliott, R. P. Membrane Permeation of Testosterone from Either Solutions, Particle Dispersions, or Particle-Stabilized Emulsions. *Langmuir* **2012**, *28*, 2510-2522.

(22) Dejmek, P.; Timgren, A.; Sjöö, M.; Rayner, M.; AB, S., Ed. 2013.

(23) Collin, N.; Candau, D.; L'oreal, Ed. 1995.

(24) Bara, I.; L'oreal, Ed. 2013.

(25) Binks, B. P.; Fletcher, P. D.; Holt, B. L.; Beaussoubre, P.; Wong, K. Selective retardation of perfume oil evaporation from oil-in-water emulsions stabilized by either surfactant or nanoparticles. *Langmuir* **2010**, *26*, 18024-18030.

(26) Fowler, J.; Syngenta, Ed. 2010.

(27) Malaquin, R. D.; Taylor, P.; Syngenta, Ed. 2010.

(28) Kralova, I.; Sjöblom, J.; Øye, G.; Simon, S.; Grimes, B. A.; Paso, K. Heavy crude oils/particle stabilized emulsions. *Adv. Colloid Interface Sci.* **2011**, *169*, 106-127.

(29) Liang, C.; Liu, Q.; Xu, Z. Dewatering Bitumen Emulsions Using Interfacially Active Organic Composite Absorbent Particles. *Energy & Fuels* **2016**, *30*, 5253-5258.

(30) Ashby, N. P.; Binks, B. P.; Paunov, V. N. Formation of giant colloidosomes by transfer of pendant water drops coated with latex particles through an oil-water interface. *Physical Chemistry Chemical Physics* **2004**, *6*, 4223-4225.

(31) Morse, A. J.; Tan, S.-Y.; Giakoumatos, E. C.; Webber, G. B.; Armes, S. P.; Ata, S.; Wanless, E. J. Arrested coalescence behaviour of giant Pickering droplets and colloidosomes stabilised by poly(tert-butylaminoethyl methacrylate) latexes. *Soft Matter* **2014**, *10*, 5669-5681.

(32) Ata, S. Coalescence of Bubbles Covered by Particles. *Langmuir* **2008**, *24*, 6085-6091.

(33) Hunter, T. N.; Pugh, R. J.; Franks, G. V.; Jameson, G. J. The role of particles in stabilising foams and emulsions. *Adv. Colloid Interface Sci.* **2008**, *137*, 57-81.

(34) Murray, B. S.; Ettelaie, R. Foam stability: proteins and nanoparticles. *Current Opinion in Colloid & Interface Science* **2004**, *9*, 314-320.

(35) Kaptay, G. On the equation of the maximum capillary pressure induced by solid particles to stabilize emulsions and foams and on the emulsion stability diagrams. *Colloids and Surfaces A: Physicochemical and Engineering Aspects* **2006**, *282–283*, 387-401.

(36) Stancik, E. J.; Kouhkan, M.; Fuller, G. G. Coalescence of Particle-Laden Fluid Interfaces. *Langmuir* **2004**, *20*, 90-94.

(37) Stancik, E. J.; Gavranovic, G. T.; Widenbrant, M. J. O.; Laschitsch, A. T.; Vermant, J.; Fuller, G. G. Structure and dynamics of particle monolayers at a liquid-liquid interface subjected to shear flow. *Faraday Discussions* **2003**, *123*, 145-156.

(38) Thompson, K. L.; Giakoumatos, E. C.; Ata, S.; Webber, G. B.; Armes, S. P.; Wanless, E. J. Direct observation of giant pickering emulsion and colloidosome droplet interaction and stability. *Langmuir* **2012**, *28*, 16501-16511.

(39) Charleux, B.; Delaittre, G.; Rieger, J.; D'Agosto, F. Polymerization-Induced Self-Assembly: From Soluble Macromolecules to Block Copolymer Nano-Objects in One Step. *Macromolecules* **2012**, *45*, 6753-6765.

(40) Canning, S. L.; Smith, G. N.; Armes, S. P. A Critical Appraisal of RAFT-Mediated Polymerization-Induced Self-Assembly. *Macromolecules* **2016**, *49*, 1985-2001.

(41) Warren, N. J.; Armes, S. P. Polymerization-Induced Self-Assembly of Block Copolymer Nano-objects via RAFT Aqueous Dispersion Polymerization. *J. Am. Chem. Soc.* **2014**, *136*, 10174-10185.

(42) Derry, M. J.; Fielding, L. A.; Armes, S. P. Polymerization-induced self-assembly of block copolymer nanoparticles via RAFT non-aqueous dispersion polymerization. *Prog. Polym. Sci.* **2016**, *52*, 1-18.

(43) Ferguson, C. J.; Hughes, R. J.; Pham, B. T. T.; Hawkett, B. S.; Gilbert, R. G.; Serelis, A. K.; Such, C. H. Effective ab Initio Emulsion Polymerization under RAFT Control. *Macromolecules* **2002**, *35*, 9243-9245.

(44) Ferguson, C. J.; Hughes, R. J.; Nguyen, D.; Pham, B. T. T.; Gilbert, R. G.; Serelis, A. K.; Such, C. H.; Hawkett, B. S. Ab Initio Emulsion Polymerization by RAFT-Controlled Self-Assembly§. *Macromolecules* **2005**, *38*, 2191-2204.

(45) Gilbert, R. G. Particle formation by self-assembly in controlled radical emulsion polymerizations. *Macromolecules* **2006**, *39*, 4256-4258.

(46) Rieger, J.; Stoffelbach, F.; Bui, C.; Alaimo, D.; Jérôme, C.; Charleux, B. Amphiphilic Poly(ethylene oxide) Macromolecular RAFT Agent as a Stabilizer and Control Agent in ab Initio Batch Emulsion Polymerization. *Macromolecules* **2008**, *41*, 4065-4068.

(47) Rieger, J.; Zhang, W.; Stoffelbach, F.; Charleux, B. Surfactant-Free RAFT Emulsion Polymerization Using Poly(N,N-dimethylacrylamide) Trithiocarbonate Macromolecular Chain Transfer Agents. *Macromolecules* **2010**, *43*, 6302-6310.

(48) Zhang, X.; Boissé, S.; Zhang, W.; Beaunier, P.; D'Agosto, F.; Rieger, J.; Charleux, B. Well-Defined Amphiphilic Block Copolymers and Nano-objects Formed in Situ via RAFT-Mediated Aqueous Emulsion Polymerization. *Macromolecules* **2011**, *44*, 4149-4158.

(49) Zhang, W. J.; D'Agosto, F.; Boyron, O.; Rieger, J.; Charleux, B. One-Pot Synthesis of Poly(methacrylic acid-co-poly(ethylene oxide) methyl ether methacrylate)-b-polystyrene Amphiphilic Block Copolymers and Their Self-Assemblies in Water via RAFT-Mediated Radical Emulsion Polymerization. A Kinetic Study. *Macromolecules* **2011**, *44*, 7584-7593.

(50) Boissé, S.; Rieger, J.; Pembouong, G.; Beaunier, P.; Charleux, B. Influence of the stirring speed and CaCl2 concentration on the nano-object morphologies obtained via RAFT-mediated aqueous emulsion polymerization in the presence of a water-soluble macroRAFT agent. *Journal of Polymer Science Part A: Polymer Chemistry* **2011**, *49*, 3346-3354.

(51) Carlsson, L.; Fall, A.; Chaduc, I.; Wagberg, L.; Charleux, B.; Malmstrom, E.; D'Agosto, F.; Lansalot, M.; Carlmark, A. Modification of cellulose model surfaces by cationic polymer latexes prepared by RAFT-mediated surfactant-free emulsion polymerization. *Polym. Chem.* **2014**, *5*, 6076-6086.

(52) Binauld, S.; Delafresnaye, L.; Charleux, B.; D'Agosto, F.; Lansalot, M. Emulsion polymerization of vinyl acetate in the presence of different hydrophilic polymers obtained by RAFT/MADIX. *Macromolecules* **2014**, *47*, 3461-3472.

(53) Truong, N. P.; Dussert, M. V.; Whittaker, M. R.; Quinn, J. F.; Davis, T. P. Rapid synthesis of ultrahigh molecular weight and low polydispersity polystyrene diblock copolymers by RAFT-mediated emulsion polymerization. *Polym. Chem.* **2015**, *6*, 3865-3874.

(54) Ning, Y.; Fielding, L.; Andrews, T.; Growney, D.; Armes, S. Sulfate-based anionic diblock copolymer nanoparticles for efficient occlusion within zinc oxide. *Nanoscale* **2015**, *7*, 6691-6702.

(55) Hatton, F. L.; Ruda, M.; Lansalot, M.; D'Agosto, F.; Malmström, E.; Carlmark, A. Xyloglucan-functional latex particles via RAFT-mediated emulsion polymerization for the biomimetic modification of cellulose. *Biomacromolecules* **2016**, *17*, 1414-1424.

(56) Cunningham, V. J.; Alswieleh, A. M.; Thompson, K. L.; Williams, M.; Leggett, G. J.; Armes, S. P.; Musa, O. M. Poly (glycerol monomethacrylate)–Poly (benzyl methacrylate) Diblock Copolymer Nanoparticles via RAFT Emulsion Polymerization: Synthesis, Characterization, and Interfacial Activity. *Macromolecules* **2014**, *47*, 5613-5623.

(57) Mable, C. J.; Thompson, K. L.; Derry, M. J.; Mykhaylyk, O. O.; Binks, B. P.; Armes, S. P. ABC Triblock Copolymer Worms: Synthesis, Characterization, and Evaluation as Pickering Emulsifiers for Millimeter-Sized Droplets. *Macromolecules* **2016**, *49*, 7897-7907.

(58) Thompson, K.; Mable, C.; Cockram, A.; Warren, N.; Cunningham, V.; Jones, E.; Verber, R.; Armes, S. Are block copolymer worms more effective Pickering emulsifiers than block copolymer spheres? *Soft Matter* **2014**, *10*, 8615-8626.

(59) Ata, S.; Davis, E. S.; Dupin, D.; Armes, S. P.; Wanless, E. J. Direct observation of pH-induced coalescence of latex-stabilized bubbles using high-speed video imaging. *Langmuir* **2010**, *26*, 7865-7874.

(60) Morse, A. J.; Giakoumatos, E. C.; Tan, S.-Y.; Webber, G. B.; Armes, S. P.; Ata, S.; Wanless, E. J. Giant pH-responsive microgel colloidosomes: preparation, interaction dynamics and stability. *Soft Matter* **2016**, *12*, 1477-1486.

(61) van Aken, G. A.; van Vliet, T. Flow-induced coalescence in protein-stabilized highly concentrated emulsions: Role of shear-resisting connections between the droplets. *Langmuir* **2002**, *18*, 7364-7370.

(62) Zhang, L.; Shi, C.; Lu, Q.; Liu, Q.; Zeng, H. Probing Molecular Interactions of Asphaltenes in Heptol Using a Surface Forces Apparatus: Implications on Stability of Water-in-Oil Emulsions. *Langmuir* **2016**, *32*, 4886-4895.

(63) Zhang, Y.; Wang, S.; Zhou, J.; Zhao, R.; Benz, G.; Tcheimou, S.; Meredith, J. C.; Behrens, S. H. Interfacial activity of non-amphiphilic particles in fluid-fluid interfaces. *Langmuir* **2017**, *DOI: 10.1021/acs.langmuir.7b00599*.

(64) Ata, S. The detachment of particles from coalescing bubble pairs. *Journal of Colloid and Interface Science* **2009**, *338*, 558-565.

(65) Thompson, K. L.; Armes, S. P.; Howse, J. R.; Ebbens, S.; Ahmad, I.; Zaidi, J. H.; York, D. W.; Burdis, J. A. Covalently Cross-Linked Colloidosomes. *Macromolecules* **2010**, *43*, 10466-10474.

For Table of Contents Use Only